Characterization of the microstructure, mechanical properties and corrosion behaviour of submicron WC-12Co coatings produced by CGS and HVAF compared with sintered bulk material

N. Cinca, O. Lavigne, H. Koivuluoto, S. Dosta, S. Conze, S. Hoehn, R. Drehmann, C. Kim, V. Matikainen, F. S. Silva, R. Jafari, E. Tarrés, A.V. Benedetti

Both as bulk material and coatings, cemented carbides currently occupy very well-established market niches and exhibit a promising future thanks to the development of compositions and manufacturing parameters. Direct comparisons of the properties of both are found only very rarely in the literature, very likely because the fields of application are complementary to each other but keep mostly separated. The current work is intended to evaluate similarities and differences in terms of microstructure and properties for two submicron WC-12 wt.%Co coatings obtained by High Velocity Air Fuel (HVAF) and Cold Gas Spray (CGS), together with a conventional sintered part. Microstructural features are discussed according to the inherent characteristics of each processing method. This covers a wide range in terms of the mechanical and thermal stresses acting on the material. While in CGS, the impacting particles do not melt, but experience extremely high plastic strain rates, the cobalt matrix is fully molten in the conventional sintering process, allowing time enough for diffusion processes. HVAF is to be placed in between, since the deposition process is characterized by a moderate heat input, leading to partial and/or full melting of cobalt, followed by rapid cooling. The microstructure and phases of the deposited coatings and bulk are characterized by using Scanning Electron Microscopy (SEM) and X-ray Diffraction (XRD). Electron Backscattered Diffraction (EBSD) investigations enable local phase distribution of Co and WC in the samples. The hardness of the alloy processed by the three different routes is investigated as well. Additionally, electrochemical corrosion measurements in NaCl media are presented to evaluate the facility for electrolyte penetration and how the degradation of the material is affected by its inherent microstructure.

1 Introduction

WC-Co is one of the most popular wear-resistant coatings, and its deposition by means of Thermal Spray technologies started in 1942 [1, 2]. This allowed overcoming certain geometrical limitations and high densities of sintered products. Some reviews by the end of last century can be found focusing on Atmospheric Plasma Spray (APS), Low-Pressure or Vacuum Plasma Spray (LPPS/VPS) or High Velocity Oxygen Fuel (HVOF) [3, 4]. At that time, however, chemical, microstructural, and phase changes that occurred during spraying were not yet fully understood. Two decades after, not only new compositions have been explored and even implemented in the market (i.e. WC–CoCr, WC–Ni, WC–'CrC'–Ni), but also new deposition techniques have emerged (i.e. High Velocity Air Fuel -HVAF-, Suspension Plasma Spraying -SPS-, Suspension HVOF -S-HVOF-, Cold Gas Spray -CGS-) resulting in a wider roadmap for this cermet material [5, 6, 7].

Nowadays, HVOF is the most widely applied technology in the market for cemented carbides and has become the industrial standard technology for their production. A step further from HVOF drives the research for higher particle velocities and lower process temperatures resulting in HVAF and CGS developments. HVAF spraying is cooler than HVOF but hotter than CGS; in HVAF, particles partially melt, while in CGS, particles remain in the solid state. Characteristic particle velocities and temperatures for each process will critically determine the final chemical composition and microstructure of the coating. Metallurgical changes of the particles within the spray jet occur over periods of milliseconds as compared of those for conventional heating of a sintered material. In any of the cases, carbide dissolution within the metal matrix, as well as cobalt phase changes (FCC-HCP) are common. The occurrence of such features with a direct comparison of properties on sintered parts can be interesting and is found only very rarely in the literature [4, 8, 9, 10].

The present study focuses on a WC-12Co alloy produced by means of HVAF and CGS. The deposited coatings contain submicronic WC and are compared with a sintered part that also contains submicron WC particles. As part of this characterization, the Electron Backscatter Diffraction (EBSD) technique has been regularly employed to determine the local phase distribution, in particular the transforming from the retained FCC to the stable HCP structure [10, 11, 12]. Less effort has been, however, dedicated to such rigorous work in coatings. The observations of Wang et al. [13] suggest that the Co binder phase becomes less tough due to numerous decarburization phases formed in the coating, and it was seen that the W_2C phases were mainly distributed in the peripheries of splats, helping to elucidate the wear mechanism of the coating. Some initial findings on how this occurs in HVAF and CGS are presented and it is evaluated how this affects hardness and corrosion properties.

2 Experimental procedure

CGS and HVAF coatings were produced with WC-12 wt.%Co cermet powders obtained by agglomeration and sintering (Fujimi Inc., Kiyosu, Japan and Durum Verschleißschutz GmbH, Willich, Germany respectively); they are characterized by containing submicronic WC particles and the powder particle sizes are in the range of -32+10 µm and -25+10 µm respectively. These were deposited onto AA 7075-T6 alloy substrates. For CGS spraying, the substrates were degreased with acetone and the surfaces were abraded with P240 SiC paper, resulting in a surface roughness (Ra) of ~1 µm. By contrast, for HVAF spraying, the substrates were only cleaned with acetone prior to spraying.

The CGS spraying of the WC-Co coatings was performed by using a Kinetics 4000/17 kW system (Cold Gas Technology, Ampfing, Germany) operating at a maximum operating pressure of 40 bar, temperature of 800 °C, and with nitrogen as the carrier gas. A WC-based nozzle (D24) was used to deposit the coatings. The parameters were optimized to improve the deposition efficiency and adhesion. Evaluation was made of pressures from 20 to 40 bar, temperatures from 400 to 800 °C, and spray distances from 10 to 40 mm. Other parameters (gun transverse speed, feed rate, and spray angle) were kept constant [14].

The HVAF spraying was carried out with M3 HVAF spray torch (Uniquecoat Technologies, Oilville, USA) with propane and compressed air as the process gases. Long combustion chamber and convergent-divergent 4L2 nozzle were used to achieve efficient melting and high particle velocities [15].

A bulk coupon obtained by conventional uni-axial pressing and sintering was produced at Hyperion Materials & Technologies (HMT) facilities; this is an ultrafine WC grain size with 12 wt.%Co, hereafter labelled as 12CoUF.

The powders and coatings were characterized by scanning electron microscopy (SEM) using a ZEISS Supra55VP microscope coupled to an X-ray microanalysis (EDS) system. Cross sections were prepared by grinding and polishing steps down to 1 µm diamond suspension. The phase composition was analysed by X-ray diffraction (XRD) using a Bruker D8 FOCUS diffractometer with LYNXEYE detector; high-resolution scans with step size of 0.01º were carried out at the region of 35–50º for the better identification of cobalt peaks and other secondary phases. The porosity of the coatings was estimated by analysing the images using Image J software, according to the ASTM E2109-01 protocol. Additionally, average WC grain size (d_{WC}) was measured by the linear intercept technique following ISO 4499-2 standard.

For the local analysis of the phase distribution, electron backscatter diffraction (EBSD) was used in FE-SEM ZEISS Crossbeam 550 using an OXFORD symmetry detector.

Vickers hardness measurements on the polished cross sections of coatings and bulks were carried out using a Emco Durascan equipment. Three indentations at 30 kgf were performed on bulks in accordance with ISO 28079. Further measurements at 5 kgf and 0.3 kgf were done to be compared with coatings and previous literature.

Corrosion measurements were conducted with a Gamry 1010E interface at 25±1 ºC in an aerated solution containing 3.56 wt.% of NaCl. A conventional three-electrode set up was used, with a graphite counter electrode and a saturated calomel electrode (SCE) as reference. The working electrode (samples with a polished surface down to 1 µm diamond suspension) was placed in a Teflon holder, leaving an exposed surface area to the electrolyte of 0.785 cm^2. The CGS sample was used as-sprayed due to its lower thickness. The open circuit potential (OCP) was recorded for respectively 24 h and 3 h for coated and bulk samples. These durations ensured OCP steady state before polarization resistance (Rp) and potentiodynamic measurements. Rp measurements were conducted at +/- 10 mV around OCP at a scanning rate of 0.167 mV/s and were followed by potentiodynamic scans from -0.150 mV_{OCP} to 0 mV_{SCE} at the same scanning rate.

3 Results and discussion

3.1 Coating microstructures

The level of heterogeneity of the CGS and HVAF coatings microstructure compared to that of the sintered part can be well noticed in Fig. 1 and Fig. 2e-j. The WC grains in the 12CoUF sample tend to touch one another forming the typical carbide skeleton, where cobalt occupies the spaces among carbides after sintering. By contrast, such contiguity cannot be observed in thermally sprayed coatings and the WC grains remain surrounded by cobalt matrix. The average WC grain size appearing in each of the microstructures shows larger values for the HVAF coating. This will contribute to the final coating properties and mainly depends on the characteristic features of the feedstock, the manufacturing process and the respective parameters, which makes comparison difficult. Together with the different WC grain size, the morphology of such grains varies in the three microstructures. In CGS, the carbide grains preserve the original angular shape of the original particles due to the solid-state nature of the process, where successful bonding and densification occur as result of plastic deformation of the feedstock, here mainly the cobalt matrix with a resulting reorganization of the carbides. The high impact on the CGS powder particles used in the process leads in part to cracking of the WC grains, see Fig. 2h where some of the cracks are marked with arrows, and to displacement of the WC and Co network. This explains a reduced linear intercept of WC and Co in the CGS coating compared to the powder (Fig. 3h). In HVAF, the thermal history of particles within the flame leads to

different degrees of decarburization and results in rounder WC grains (Fig. 2j). Finally, the Ostwald Ripening process drives the coarsening of WC grains during liquid phase sintering in 12CoUF [4, 16].
The results from the EBSD analysis are illustrated in Fig. 3 a-g. In general, no preferred orientations for WC and Co grains could be identified. The EBSD analysis of the powder particles and 12CoUF confirms the good homogeneity of WC and Co. In the starting material, Co is present as small grains, showing the IPF-Z (Inverse Pole Figure) illustration in Fig. 3f,g. In contrast, the Co matrix in 12CoUF is characterized by huge Co grains larger >> 10 µm (not illustrated here, but similar to [11, 12]), despite homogeneous distribution and similar to the powder linear intercept d50 of 96 nm. The investigations on coatings resulted in a determination of the WC grains; however, the binder did not provide any electron diffraction patterns. This can be attributed to a high proportion of deformation in the binder phase. It corresponds to residual stress type-3, which contributes to the broadening of the peaks in the XRD pattern, as can be observed in Fig. 4.

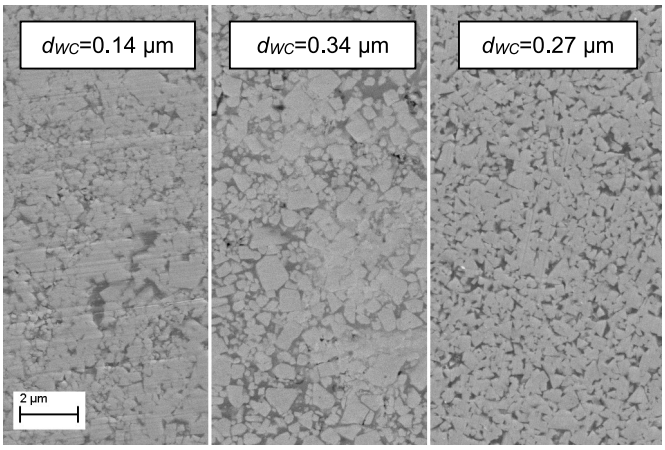

Figure 1. SEM micrographs showing the microstructure of the CGS coating (left), HVAF coating (middle) and 12CoUF sintered part (right).

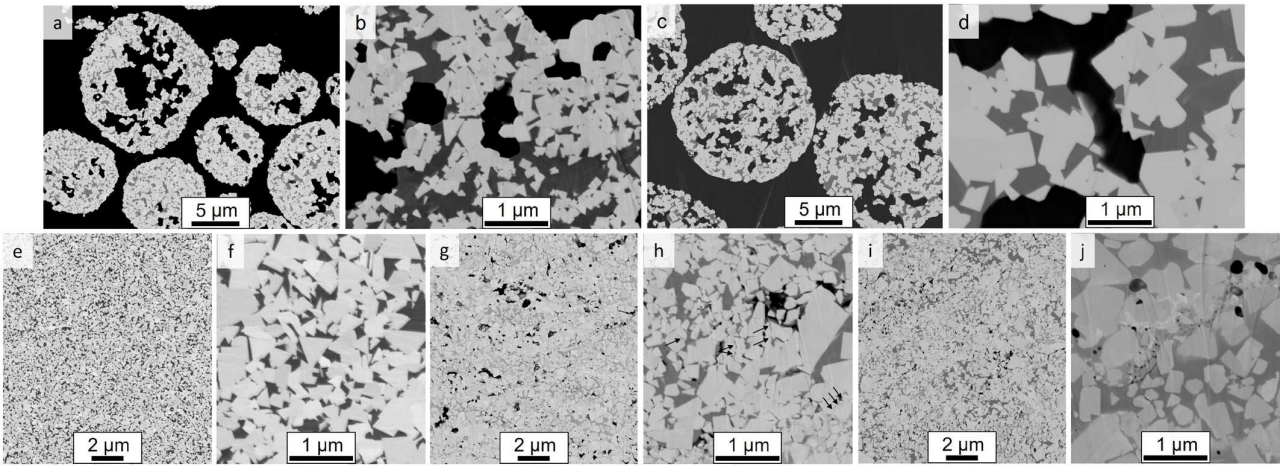

Figure 2. SEM micrographs showing the microstructure of (a-b) CGS powder, (c,d) HVAF powder, (e,f) Bulk, (g,h) CGS coating (arrows mark cracks) and (i,j) HVAF coating

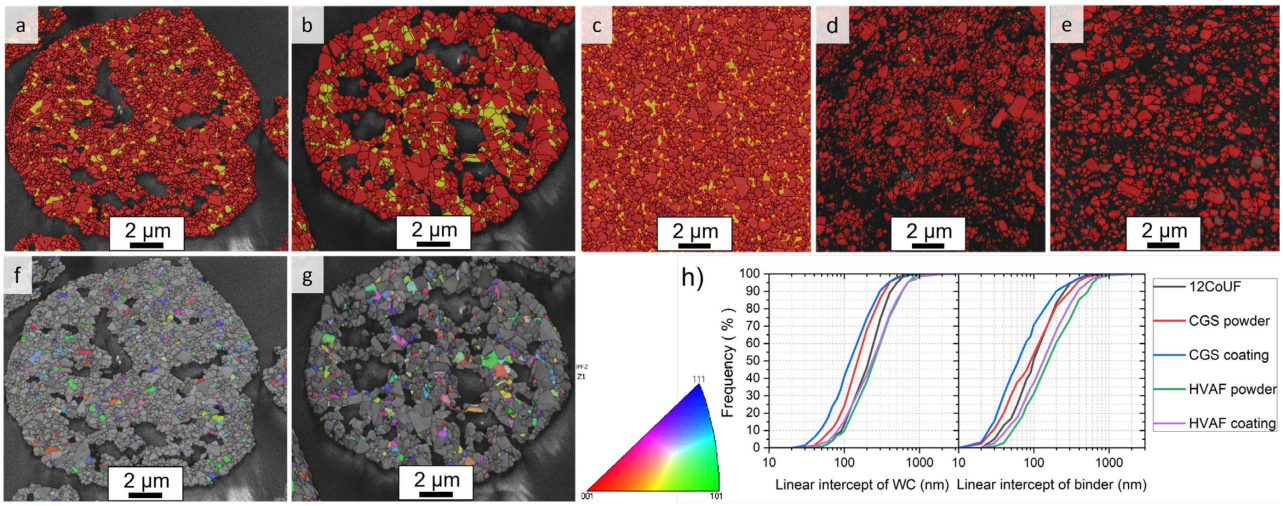

Figure 3. (a-g) EBSD results showing the (a-e) the grain boundary and phase composition with (red) WC and (yellow) FCC Co and (f,g) orientation mapping (inverse pole figure in z-direction, IPF-Z) from FCC Co of (a,f) CGS powder, (b,g) HVAF powder, (c) 12CoUF, (d) CGS coating and (e) HVAF coating. (h) Linear intercept of WC and binder.

The cobalt matrix of the HVAF coating appears lighter in the SEM micrographs due to the WC dissolution and high temperature reactions. Although the flame and resulting particle temperature in HVAF is typically lower than that of HVOF, reactions with oxygen can still occur to a certain extent, resulting in other carbide stoichiometries, as observed in X-ray diffractograms of Fig. 4b. The present identification of the HVAF coating cannot exclude the presence of any other phase since peaks tend to be broadened, convoluted or shifted in position [4]. When sprayed by CGS, no secondary phases can be primarily observed, but the broadening of peaks can be indicative of the accumulated strain upon particle impingement [17]. This can be different from the HVAF coating, where broadening might be rather attributed to nanocrystalline phases and amorphization as result of non-equilibrium phenomena. In addition, FCC-HCP Co transformations are also worth mentioning. CGS and HVAF powders are agglomerated and sintered, so the high temperature FCC structure of cobalt is retained when the binder solidifies, whereas HCP may locally form in regions of existing residual stresses (Fig. 4a). By contrast, the 12CoUF powder, which is just agglomerated, only exhibits the low temperature stable HCP phase; after processing, the FCC appears (Fig. 4b). The occurrence of HCP in the CGS coating can be attributed to the strain-induced transformation from FCC to HCP structure; the high-resolution scans within the 35–50° (two theta) region compared to those of the original powders determined that this occurs in CGS as result of plastic deformation during particle impingement.

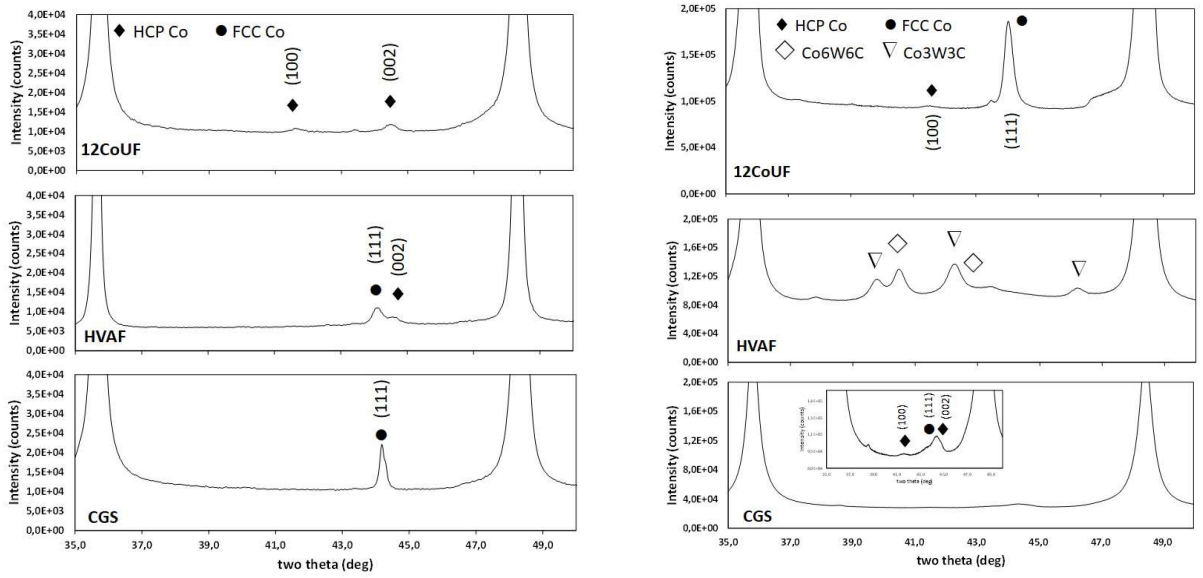

(a) (b)

Figure 4. X-ray diffraction of: (a) powders and (b) CGS, HVAF and 12CoUF samples (high-resolution scans of 35–50°). Identification with XRD patterns with PDF-ICDD- 05-0727 for Co-HCP and 015-0806 for Co-FCC.

3.2 Hardness

The different powder type processing, spraying techniques and processing parameters, inevitably lead to certain inconsistency of coating properties even when the nominal composition is the same [4]. The complex nature of deposits with different amounts of porosities, oxidation and other chemical and metallurgical changes lead to the relatively low hardness values of thermally sprayed coatings in comparison to cemented carbides produced by other manufacturing methods. For example, compared to conventional pressed and sintered WC-Co parts, which typically exhibit hardness values in the range of ~750 to 2250 HV, thermally sprayed ones range from ~795 to 1568 HV [10]. In the present case, this is illustrated by the 12CoUF sample exhibiting average values larger than those of CGS and HVAF. The higher hardness of the CGS coating compared to the HVAF can be most likely attributed to the smaller WC grain size and the strain hardening of the Co matrix.

Table 1. Hardness values of samples.

kgf	***CGS***	***HVAF***	***12UF***
0.3	1419 ± 93	1153 ± 58	-
5	-	1066 ± 35	1805 ± 12
30	-	-	1743 ± 15

3.3 Corrosion performance

The overall corrosion process of WC-Co alloys is very complex due to their heterogeneous microstructure as well as the galvanic interaction between the two phases. In bulk cemented carbides, the WC grain size, binder content and nature have been found to have a large influence on the electrochemical behaviour of these materials [18, 19]. The pH of the electrolyte is also of paramount importance as the cobalt matrix is known to be very sensitive to dissolution in acidic media while WC tends to be dissolved in alkaline media. The further complexity imposed in coatings as result of the porosity occurrence intersplat boundaries and likely undesired phases, introduce further paths for electrolyte penetration.

In the present study, the 3.56 wt.% NaCl electrolyte presents a slightly acidic pH of 6.5. As shown in Table 2 and Fig. 5, the highest E_{corr} value corresponds to the CGS coating, probably because of some level of oxidation of the cobalt phase on the non-polished surface, which could contribute to the increase of the potential. The measurements onto the as-sprayed HVAF coating were not possible because of its high resistivity most likely due to the presence of a thicker oxide layer on the surface generated by the deposition process. The polished HVAF coating shows higher polarization resistance and lower corrosion current density compared to the other samples that could be due to the presence of remaining oxides, Co_xW_xC compounds and some level of amorphization of the microstructure [20]. The polarization resistance of the CGS sample may also be influenced by the residual stresses inherent to the CGS technique, which can increase the activity of the coating. The electrochemical behavior of the bulk sample is the result of its specific microstructure (binder content and nature and WC grain size) and the presence of tensile residual stresses in the binder resulting from the sintering process.

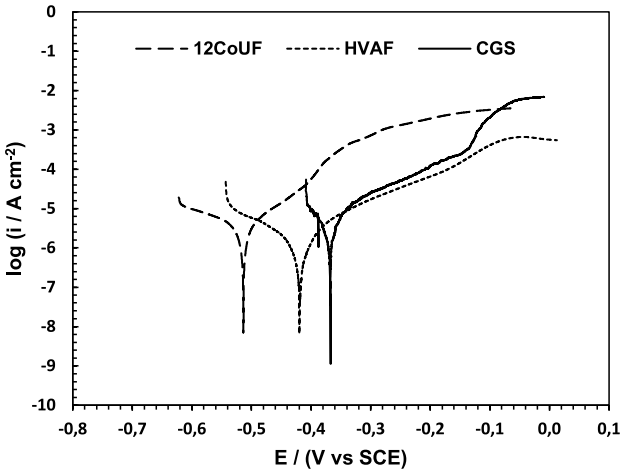

Figure 5. Potentiodynamic curves for CGS (unpolished), HVAF (polished) and 12CoUF (polished) samples in 3.56 wt.% NaCl (pH 6.5)

Table 2. Corrosion potential and polarization resistance of the three samples.

	Ecorr (V vs SCE)	***Rp (kΩ cm²)***
HVAF (polished)	-0.420	7.2±0.4
CGS (unpolished)	-0.367	2.8±0.3
12CoUF (polished)	-0.510	2.7±0.1

4 Conclusions

The WC-12 wt.%Co coatings processed by means of HVAF and CGS exhibit higher heterogeneity than the conventional pressed and sintered sample. The three final materials were obtained with ultrafine WC grain size, but with significantly different features in terms of carbide size distribution, angularity and dissolution. The CGS process leads to more WC angularity and grain size refinement due to fracture upon impact, while HVAF is rather featured by WC roundness and presence of other stoichiometric carbides due to dissolution, which is visible by SEM and EBSD evaluations. Additionally, the cobalt phase changes have also been identified by XRD, with the well-known retention of the metastable FCC phase in the sintered material and the partly strain-induced transformation from FCC to HCP in CGS. All this results in the illustrated different hardness values and electrochemical corrosion performance. The latter is also very likely influenced by the presence of tensile residual stresses.

Acknowledgements

The authors would like to acknowledge the Thermal Spray Center (CPT) in the University of Barcelona for the use of Cold Gas Spray facilities to produce the CGS coatings.

Literature

[1] R. J.K. Wood, Tribology of thermal sprayed WC–Co coatings, *Int. J. Refract. Metals Hard Mater.,* 28 (2010) 82–94.
[2] L. Berger, Hardmetals as thermal spray coatings, *Powder Metallurgy* 50:3 (2007) 205-214
[3] S. F. Wayne, S. Sampath, Structure/property relationships in sintered and thermally sprayed WC-Co, *J. Thermal Spray Technol.*, 1 (1992) 307-315.
[4] H.L. de Villiers Lovelock, Powder/Processing/Structure Relationships in WC-Co Thermal Spray Coatings: A Review of the Published Literature, *J. Thermal Spray Technol.*, 7 (1998) 357-373.
[5] A. Vardelle et al., The 2016 Thermal Spray Roadmap, *J. Thermal Spray Technol.*, 25 (2016) 1376-1440.
[6] L-M Berger, Application of hardmetals as thermal spray coatings, *Int. J. Refract. Metals Hard Mater.,* 49 (2015) 350–364.
[7] M.Couto, S.Dosta, J.M.Guilemany, Comparison of the mechanical and electrochemical properties of WC-17 and 12Co coatings onto Al7075-T6 obtained by high velocity oxy-fuel and cold gas spraying, *Surf. Coat. Technol.*, 268 (2015) 180-189
[8] P. L. Kuhanen et al.,: Proc. TS'93: 'Vortrage und Posterbeitrage der Thermischen Spritzkonferenz '93', Aachen, Germany; DVS-Ber., 1993, 152, 100–102 (Deutsche Verlag für Schweißtechnik, Du¨ sseldorf).
[9] J.A. Picas et al., Microstructure and wear resistance of WC–Co by three consolidation processing techniques, *Int. J. Refract. Metals Hard Mater.,* 27 (2009) 344–349.
[10] R. Ahmed et al., Sliding wear of conventional and suspension sprayed nanocomposite WC-Co coatings: An invited review, *J. Thermal Spray Technol.*, 30 (2021) 800-861
[11] K.P. Mingard et al., Some aspects of the structure of cobalt and nickel binder phases in hardmetals, *Acta Mater.,* 59 (2011) 2277-2290.
[12] J. M. Marshall et al., Binder phase structure in fine and coarse WC–Co hard metals with Cr and V carbide additions, *Int. J. Refract. Metals Hard Mater.,* 40 (2013) 27–35
[13] H. Wang et al., Abrasion Resistance Enhancement of Ultrafine-structured WC-Co Coating Fabricated by using in situ Synthesized Composite Powder, *J. Mater. Sci. Technol.*, 29:11 (2013) 1067-1073.
[14] F.S. da Silva et al., Corrosion behavior of WC-Co coatings deposited by cold gas spray onto AA 7075-T6, *Corrosion Sci.* 136 (2018) 231–243.
[15] V. Matikainen et al. , Effect of Nozzle Geometry on the Microstructure and Properties of HVAF-Sprayed WC-10Co4Cr and Cr3C2-25NiCr Coatings, *J. Thermal Spray Technol.*, 27 (2018) 680-694.
[16] J. Garcia et al., Cemented carbide microstructures: a review, *Int. J. Refract. Metals Hard Mater.,* 80 (2019) 40-68.
[17] S. Dosta et al., Plastic deformation phenomena during cold spray impact of WC-Co particles onto metal substrates, *Acta Mater*. 124 (2017) 173e181
[18] L. Zhang et al., Electrochemical corrosion behaviors of straight WC–Co alloys: Exclusive variation in grain sizes and aggressive media, *Int. J. Refract. Metals Hard Mater.* 57 (2016) 70–77
[19] Y. Zheng et al., Corrosion-Induced Damage and Residual Strength of WC-Co,Ni Cemented Carbides: Influence of Microstructure and Corrosion Medium, *Metals* 2019, 9, 1018; doi:10.3390/met9091018
[20] M. Magnani et al., Influence of HVOF parameters on the corrosion and wear resistance of WC-Co coatings sprayed on AA7050 T7, *Surf. Coat. Technol.* 202 (2008) 4746–4757.